Estuaries and Coasts (2023) 46:494–511
https://doi.org/10.1007/s12237-022-01133-2

Quantifying the Effects of Floating Oyster Aquaculture on Nitrogen Cycling in a Temperate Coastal Embayment

Micheline S. Labrie[1] · **Miles A. Sundermeyer**[1] · **Brian L. Howes**[1]

Received: 18 February 2022 / Revised: 3 October 2022 / Accepted: 4 October 2022 / Published online: 28 October 2022

Abstract

Estuaries worldwide are increasingly degraded by anthropogenic nitrogen (N) inputs, primarily from their watersheds. In southeastern Massachusetts, several municipalities are implementing floating oyster aquaculture in their estuaries as a means of increasing N removal through assimilation into oyster biomass, sediment burial, and enhanced sediment denitrification. Denitrification associated with floating oyster aquaculture was quantified in a Cape Cod tidal salt pond to determine the effectiveness of this non-traditional approach. Exchange of dinitrogen gas, oxygen, and nutrients between water column and sediments was measured inside and outside of sediment areas affected by oyster biodeposits. Enhanced sediment denitrification was observed during each of the 3 years of the study, with the degree of enhancement varying between seasons and years; enhanced denitrification totaled 2.8, 2.4, and 3.3 g N_2-N m^{-2} (265%, 309%, and 388% of background) for summer and fall months of 2016, 2017, and 2018, respectively. Continued enhanced denitrification each following spring contributed additional N removal, averaging 1.4 g N_2-N m^{-2} (449% of background) beyond previous summer and fall enhancements. Differences in enhanced denitrification were attributable to interannual and seasonal differences in N deposition, bottom water dissolved oxygen, and nitrate + nitrite concentrations. Oyster biomass within each bag and the pond varied by year resulting in differences in the spatial extent and intensity of N biodeposition to surficial sediments, and level of enhanced denitrification. This shows that such information is necessary to assess the efficacy of using floating oyster aquaculture to reach N reduction goals within eutrophic coastal embayments typical of southeastern Massachusetts.

Keywords *Crassostrea virginica* · Suspended shellfish aquaculture · Nitrogen cycling · Denitrification · Biodeposition · Estuarine restoration

Introduction

Coastal systems in the temperate zone around the globe are being polluted by nitrogen (N) entering from their watersheds as a result of anthropogenic activity (Howarth et al. 2002). Anthropogenic N enters coastal ecosystems primarily as dissolved inorganic N (DIN) and stimulates primary productivity, which can lead to phytoplankton blooms and a cascade of negative ecological effects. In response to nationwide water quality concerns, the federal Clean Water Act (CWA) (Sect. 303 (d)) established regulatory measures to restore and maintain the overall health of the nation's waters. A total maximum daily load (TMDL) was set for each pollutant within a system not meeting CWA standards. Municipalities are currently grappling with the need to reduce N loading in estuaries to meet these regulatory TMDLs. Traditional wastewater collection and treatment is expensive; therefore, researchers have been intensively working to develop non-infrastructure approaches for removing N before it reaches estuarine waters or to enhance the removal of N within the estuary itself. Similarly, interest in nutrient trading programs has increased in recent years. As a result, environmental managers must quantify N removal for a variety of alternate approaches if they are to be implemented as a N management tools (Ray et al. 2021; Rose et al. 2021).

Oyster aquaculture is being investigated as a sink for N that has reached the estuary from the surrounding airshed

Communicated by Eric N. Powell

✉ Micheline S. Labrie
mlabrie@umassd.edu

[1] Department of Estuarine and Ocean Sciences, School for Marine Science and Technology, University of Massachusetts Dartmouth, 706 South Rodney French Blvd, New Bedford, MA 02744, USA

and watershed (Ayvazian et al. 2021). Bivalves affect biogeochemical cycling by filtering out phytoplankton and other particulate matter, thus increasing water clarity. Particulate matter captured on the gills can be rejected as pseudofeces, or ingested, digested, and released as feces (Newell and Jordan 1983), both of which increase deposition to bottom sediments. The majority of the digested organic N is assimilated into oyster tissue and shell for maintenance and growth, and some amount is excreted, primarily as ammonium (NH_4^+; Bayne and Hawkins 1992). Assimilation and subsequent oyster harvest is a potential permanent N removal pathway as the removed oysters store N and make it unavailable for uptake by phytoplankton and microbes.

Pseudofeces and feces, collectively called biodeposits, are denser than ambient suspended particulates. Once released to the water column, biodeposits quickly settle to the sediment surface, where the organic N in the biodeposits may be permanently buried in the anoxic sediment layer or regenerated as NH_4^+. Ammonium in the oxic sediments can diffuse to the water column or be available for sediment nitrifying bacteria. Nitrifying bacteria derive energy through the metabolic process of nitrification. Nitrification is a two-step process that requires the presence of oxygen to transform NH_4^+ into nitrite and then nitrate (NO_3^-); it occurs in the upper oxic sediment layer (Fenchel et al. 1998). The NO_3^- from nitrification can either be released into the overlying water column or can diffuse to the anoxic sediment layer where it is available to denitrifying bacteria.

Denitrification is limited in sediments with free oxygen, but occurs in anoxic zones if NO_3^- is present. Denitrification generates energy as denitrifying microbes consume organic matter and convert NO_3^- to dinitrogen gas, which escapes the aquatic system into the atmosphere. Nitrification provides a NO_3^- source for denitrification. Therefore, nitrification and denitrification typically occur as coupled processes (termed coupled nitrification–denitrification; CND) in shallow-water estuaries (Hamersley and Howes 2005). Many factors contribute to the potential for CND, including the level of overlap between oxic and anoxic zones in the sediment (Fenchel et al. 1998). In contrast, direct denitrification typically occurs where NO_3^- is available in waters overlying redox stratified sediments, and NO_3^- diffuses into the sediments to the anoxic layer to support denitrification (Piehler and Smyth 2011). Direct denitrification depends mainly on the availability of water column NO_3^-.

Two other N transformations that have received less attention are dissimilatory reduction of NO_3^- to ammonium (DNRA) and anaerobic ammonium oxidation (anammox). DNRA is the direct conversion of NO_3^- to ammonium, and may compete with denitrification for NO_3^-; it is a microbial process that conserves N within a system and therefore is not part of N removal. DNRA has been reported in shallow-water estuaries in Texas, North Carolina, and Virginia (An and Gardner 2002; Smyth et al. 2013; Lunstrum et al. 2018), and can be associated with oyster reefs and off-bottom oyster culture. Anammox is a microbial-mediated process in which ammonium and nitrite are converted directly to dinitrogen gas in the absence of O_2. Anammox is a potential N loss pathway similar to denitrification, but it is not believed to play a large role in shallow-water polyhaline estuaries (Rich et al. 2008); studies conducted in MA and NY suggested that anammox contributed < 10% of N_2 production (Engström et al. 2005; Koop-Jakobsen and Giblin 2009). To the extent that anammox occurs at oyster sites, the N_2 generated would be captured with the N_2 from denitrification in assays that quantify N_2 production as the measure of microbial N removal.

Oyster aquaculture may increase net denitrification by increasing NH_4^+ production when bottom water dissolved oxygen (DO) levels are sufficient to maintain an oxygenated surficial sediment layer. Denitrification and denitrification efficiency (generally described as N_2 production relative to total N remineralization) appears to be site-specific, and published data are quite variable (Kellogg et al. 2014). The observed variability in denitrification rates and efficiencies is likely attributable to differences in site-specific environmental conditions, aquaculture management practices, and techniques used to measure denitrification. A more quantitative understanding requires collecting data across different settings to identify patterns and determine what features are related to oyster aquaculture and enhanced denitrification. At present, given the significant N management effort, data specific to embayments characteristic of southeastern Massachusetts (i.e., eutrophic shallow-water depositional systems) is needed.

Several previous studies have measured nutrient and N_2 flux rates associated with oyster aquaculture, but the systems studied to date have significant differences compared to southeastern MA embayments including depth, hydrodynamics, and water column particulate composition, as well as aquaculture type (e.g., species and gear; Kellogg et al. 2014; Humphries et al. 2016; Lunstrum et al. 2018). In the present study, we quantified N cycling relative to floating oyster aquaculture, specifically, the potential for enhanced denitrification, and the relationship between N deposition and environmental conditions affecting denitrification. We hypothesized that (1) biodeposition resulting from floating oyster aquaculture would enhance sediment denitrification rates, (2) labile biodeposits would continue to enhance denitrification rates after oyster removal from the system and into the following spring, and (3) the degree of enhancement would be a function of both bottom water DO and the amount of biodeposits settling to the sediment surface.

Methods

Study Site and Oyster Aquaculture Characteristics

Lonnie's Pond (Orleans, MA; 41.7693° N, – 69.9768° W), a eutrophic shallow-water depositional system, was used to examine the effect of oyster aquaculture on N cycling previously described in Labrie et al. (2022). Lonnie's Pond (0.06 km^2) is a drown kettle pond with an average depth of 3.0 m; it receives surface water flow via a freshwater stream along the southwest shore (stream enters 50 m from nearest edge of the floating bags) and tidal input through an inlet on the southeast section of the pond (Fig. 1a). It is a tributary to the Pleasant Bay Estuary (lagoon) located on the eastern-most shore of Cape Cod on the Atlantic Ocean. Lonnie's Pond and other tributaries to the Pleasant Bay Estuary are impaired by excessive N inputs from their watershed. Findings of the MA Estuaries Project (Howes et al. 2006) indicated that the N load to Lonnie's Pond would need to be lowered by 300 kg N $year^{-1}$ (33% of the N loading to its watershed) to mitigate impairment, with other tributaries to the Pleasant Bay Estuary also requiring similar reductions. In 2016, floating oyster aquaculture was established in Lonnie's Pond to test its use for N removal through N assimilation with oyster harvest and enhanced sediment denitrification. Two oyster cohorts, first (0 +) and second year (1 +), were deployed in spring or early summer 2016–2018 and harvested or overwintered in late fall of the same year. Aquaculture deployments included 200,000 oysters (800 bags), 600,000 oysters (1012 bags), and 2.1 million oysters (1515 bags) in 2016, 2017, and 2018, respectively. First-year oyster seed (2–3 mm) was deployed in 0.75-mm mesh modified spat bags with attached floats, and then size-sorted and redeployed in 6-mm mesh bags once shell lengths reached approximately 12 mm. The 6-mm diamond mesh bags consisted of high-density polyethylene (Intermas brand; 1 m × 0.5 m) and were made positively buoyant with two attached foam floats. Floating bags were routinely cleaned, and oysters were size graded to maximize food availability to promote biodeposition and oyster growth. Bags were flipped in place periodically (weekly to bi-weekly) to reduce biofouling and to redistribute oysters within each bag. Aquaculture plots and the degree of overlap across the 3 years of the study are shown in Fig. 1b.

Whole bag oyster weights were determined for each bag upon deployment and removal from the pond at the end of the growing season. Total biomass increase over the deployment period was determined by weight increase. In addition, 25–30 oysters from each aquaculture plot and cohort were collected upon deployment in early spring and removal in late fall for determination of whole oyster wet weight, dry tissue weight (DTW), dry shell weight, and N content. Oyster tissue and shell were dried for a minimum of 72 h at 60 °C. Nitrogen content of tissue and shell and the mass of N removed at the end of the growing season were determined following procedures described by Kellogg et al. (2013) and Reitsma et al. (2014) using elemental analysis (measured at Boston University's Stable Isotope Laboratory) following standard procedures. Biomass increase was multiplied by percent N content of whole oysters to determine net N assimilation at time of removal from Lonnie's Pond.

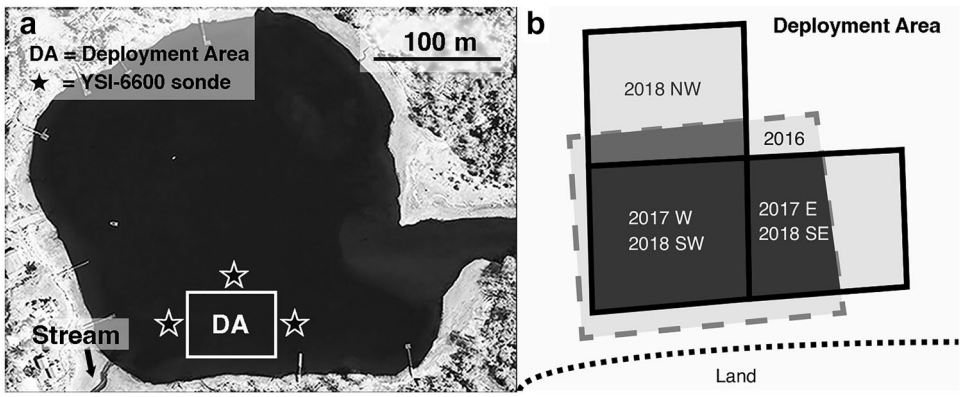

Fig. 1 Satellite image of Lonnie's Pond, Orleans (**a**). Composite diagram of 2016–2018 deployment areas showing relative size and position of aquaculture plots. The 2016 deployment area held 8 longlines, installed ~ 3 m apart with 2 rows of 50 bags on each longline. 2017 and 2018 deployment areas were divided into square plots (378 m^2) each holding 30 rows of 17 bags; this higher density layout resulted in a 50% increase in the number of bags per unit area compared to 2016. The 2018 SW and SE plots were the same as the 2017 W and E plots, respectively. The 2018 NW plot was 2.8 m water depth: 1 m deeper than the other areas (**b**)

Field Sampling and Water Chemistry

Time series measurements of DO, temperature, and salinity were made using moored YSI-6600 sondes during the 2016–2018 growing seasons. Sensors were 30 cm above the sediment surface within the oyster deployment area and approximately 4 m to its east and west (total depth ~ 1.8 m) to measure oxygen conditions near the sediment surface. A fourth mooring was placed approximately 4 m north of the deployment area in surface waters ~ 3 m above the sediments (total depth ~ 3.5 m) to monitor surface/mixed-layer water quality outside the influence of oyster biodeposit degradation in the sediments. Measurements were recorded every 15 min and sensors calibrated bi-weekly with triplicate samples for DO by Winkler (Oudot et al. 1988). Water quality sampling was conducted prior to aquaculture deployment and throughout the oyster growing season, and also included collecting grab samples and flow measurements of the stream entering the pond. Bi-weekly water quality sampling began in June 2016, corresponding with oyster deployment, and in April in 2017 and 2018.

Water depth, Secchi depth, temperature, and DO were recorded during water column sampling. Whole water was held in acid-leached 1-L brown HDPE bottles for laboratory collection of particulate carbon (C) and N, and 60 mL subsamples were field filtered (0.2 µm) into acid-leached polyethylene bottles for analysis of dissolved inorganic and organic N and P constituents. Water samples were stored dark on ice for transport to the Coastal Systems Analytical Facility at UMassD/SMAST. Filtered samples were assayed for ammonium (NH_4^+) following the indophenol/hypochlorite method (Scheiner 1976) and ortho-phosphate (Murphy and Reilly 1958) within 24 h of collection. The remaining sample was frozen (− 20 °C) until assayed for combined nitrate + nitrite ($NO_x^- = NO_2^- + NO_3^-$) by cadmium reduction on a QuikChem 8000 Lachat auto analyzer (Wood et al. 1967) and dissolved organic N by persulfate digestion (D'Elia et al. 1977). Particulate organic C and PON were determined by filtering whole water through pre-combusted 25-mm Whatman glass fiber filters within 24 h of collection, drying (65 °C), and assayed using a Perkin Elmer Series II CHN elemental analyzer (Kristen 1983).

Sediment Core Collection and Incubation

The spatial extent of biodeposition to sediments (biodeposit area) from overlying floating oyster bags was determined using in situ biodeposition rates (standardized to a 1-g dry tissue weight oyster) measured over a range of water quality conditions, and a site-specific particle advection model (Labrie et al. 2022). To measure biodeposition, biodeposit traps (based on a design developed by Higgins et al. 2013) were secured directly below individual unmodified floating bags in Lonnie's Pond for 24–72 h to capture biodeposits settling from the bags. A control biodeposit trap was deployed during each event to determine background particle settling rates, which was then subtracted from measured total deposition rates to yield biodeposition rates. Biodeposited C and N masses were based on field biodeposition rates and C and N content of collected biodeposits as determined by elemental analysis. Per the particle advection model described in Labrie et al. (2022), for 2017 and 2018, oyster biodeposits were advected by horizontal currents upon release from floating oyster bags. Measured horizontal velocities (Acoustic Doppler Current Profiler (ADCP); Aquadopp Profiler HR 2 MHz ADCP, Nortek USA Inc., Boston, MA, USA), biodeposit settling rates, and water column depth were used to predict horizontal displacement of biodeposits settling to the sediment surface relative to the biodeposit source (i.e., oysters within the floating bags). The upward-facing ADCP was deployed in Lonnie's Pond in October 2017 and July and October 2018 over multiple tidal cycles to capture seasonal variability. During each event, the ADCP was mounted on a 12-mm thick rectangular base and was deployed directly below or next to (1.5 m north) the floating bags. Individual horizontal displacements were summed across a 2-D grid to estimate biodeposition intensity relative to the location of the floating bags and sediment core collections. The summed displacements were used to determine the degree to which sediments received labile nutrient-rich biodeposits. In particular, N deposition (biodeposition N + background N) relevant to each core location was predicted using the biodeposit model (N biodeposition standardized to a 1-g dry tissue weight oyster) plus inputs due to background settling of N (based on measured particulate organic N, total depth, and a turnover of 15.5% per day; Lohrenz et al. 1987), all referenced to a 2-D grid of oyster dry tissue weights (representing the floating oyster bags). In the present study, for 2016 only, biodeposit area was determined using the 2017 predicted ratio between modeled biodeposit area and deployment area. A maximum distance of biodeposit displacement was then determined based on barotropic mean velocity, maximum water column depth, and biodeposit settling velocity.

Per Labrie et al. (2022), the particle advection model was verified by comparing predicted C deposition with measured sediment oxygen demand (SOD) rates assuming that the molar ratio of CO_2:O_2 during respiration was 1:1. Findings indicated that predicted C deposition was positively correlated with measured SOD. The implication was that the spatial extent of biodeposition to the sediments (i.e., organic C deposition) was largely accounted for by on-site C mineralization, and therefore that particle transport beyond the biodeposit area was minimal. In the present study, predicted N deposition was compared with measured N remineralization.

Determination of the biodeposit area was used to select coring locations affected by biodeposit loading, vs. those

receiving only background (non-oyster) deposition. Sediment cores collected outside of the biodeposit area represent background benthic flux rates and are referred to as control sediments or control cores, while sediments collected within the biodeposit area are referred to as treated sediments or treated cores.

Twelve to sixteen cores were collected on each sediment collection date depending on the area and heterogeneity of sediments being examined. In general, core locations were distributed to capture potential variation in nutrient flux rates throughout the biodeposit area, as well as the variability of control sediments. Sampling within the biodeposit area aimed to capture differences attributable to different oyster sizes, ages, and stocking densities, as well as the amount of time oysters were deployed. In 2016 only, sediment cores were only collected directly below the floating bags or beyond the maximum biodeposit deployment distance. Sediment collections began after at least 30 days of oyster deployment and continued to capture seasonal variations focusing on periods of high oyster and sediment metabolic activity in late summer, early fall, and early spring (2017 and 2019). July, August, and September incubations captured warmer summer water conditions and peak temperatures and biodeposition rates, whereas October incubations captured conditions of cooler more oxygenated bottom water and maximum oyster biomass. Finally, early spring incubations were conducted prior to oyster deployment to capture any residual effects of the prior year's accumulated biodeposits that overwintered as temperatures began to warm and sediment metabolism increased.

Intact sediment cores were collected by SCUBA diver in core tubes (15 cm i.d., 30 cm height, 15 cm of sediment) and were immediately transported at in situ temperature by boat to a nearby field laboratory for incubation in pre-equilibrated insulated water baths. Headspace water was replaced with filtered (0.22 µm) water (e.g., "fill water") from the core site, aerated, and mixed at speeds that replicated in situ conditions without inducing resuspension. Incubation baths and core headspace water were held within 1–2 °C of in situ temperatures. Following incubations, sediment cores were sub-sampled (upper 2 cm sediment, 66.37 cm^3) for N content by drying (60 °C drying oven, 72 h) and homogenizing with mortar and pestle, and analyzed using a Perkin Elmer 2400 elemental analyzer.

Time series measurements of DO in headspace water were made through a port in the gas tight top using a YSI ProDO optical probe and DO was kept > 3 mg L^{-1}. Oxygen uptake rate was determined by linear regression of the time course of headspace DO concentrations ($N \geq 5$). Parallel time series measurements of NH_4^+, ortho-phosphate, NO_x^-, and dissolved organic N were conducted over a 16- to 18-h period under dark conditions, mimicking the low bottom water light levels at the coring site. An experiment to confirm the use of dark incubation was conducted under in situ light (measured as 43–88 µE m^{-2} s^{-1}) and dark conditions in late September and no difference was found between DO uptake under low in situ light and dark incubation ($t = 1.151$, df = 15, $p = 0.268$). September cores were collected during a period of reduced phytoplankton biomass compared to spring and summer highs; however, the lack of difference between light and dark incubations indicates that light availability at the sediment surface was not sufficient to support benthic photosynthesis. Similar to DO, nutrient uptake/release rates were based on linear regression ($N \geq 5$) of constituent concentration. The effects of the two treatments (treated vs. control) were examined by season and project year, and their interactions on SOD and nutrient fluxes were determined using a 3-way ANOVA. Data were transformed to meet assumptions of normality and equality of variance when necessary. A Tukey–Kramer correction was applied to adjust the *p*-values for multiple comparisons of treatments with unequal sample sizes (cores). Outlier analysis was performed prior to treatment comparison; cores were removed if surficial sediments were sulfidic or if a large burrowing organism, such as a quahog, was found upon breakdown of the experiment.

After completing DO and nutrient time series measurements, cores were again capped gas tight with a water headspace for time series measurements of N_2 production. Measurements did not differentiate between coupled nitrification–denitrification, direct denitrification, or anammox; therefore, N_2 production was used as a measure of total denitrification. Headspace samples were collected in 40-mL glass serum vials and preserved with 0.25 mL of 25% hydrochloric acid and capped with butyl rubber stoppers (Charoenpong et al. 2014). DO concentrations within the headspace were not allowed to drop below 3 mg L^{-1}.

Denitrification was determined from linear regression of time series measurements of N_2 excess as assayed using a Multicollector Isotopic Ratio Mass Spectrometry (MC-IRMS with GV IsoPrime analyzer; Charoenpong et al. 2014). N_2 produced by denitrification is precisely detected from its ratio with the naturally occurring inert gas argon. Samples were pumped through a gas permeable membrane to extract gas into the mass spectrometer inlet. The inlet was fitted with cryogenic traps to remove water vapor and CO_2. Sample gas was analyzed for masses 28 (N_2) and 40 (Ar) for determining the N_2 to Ar ratio. Calibration used a certified reference gas mixture of argon, N_2, and oxygen. A one-tailed *t* test was used to assess the difference between denitrification rates in sediments from biodeposit affected versus background (control) areas, and oyster-mediated enhanced denitrification was determined as the difference between rates in treated sediments and control sediment areas.

Results

Oyster Growth and N Assimilation

Deployment and removal dates for each year, and dry tissue weights relative to bag count and deployment surface area, are shown in Table 1. Oysters were deployed for 175, 230, and 241 days (first date of deployment to last day of recovery) in 2016, 2017, and 2018, respectively, yielding a live whole oyster biomass increase through growth of 8,458, 8,769, and 10,079 kg, respectively. Nitrogen content of whole oysters was 0.31% by mass (live whole oyster biomass) for 0 + and 1 + oysters for all years except 2018; N content of 1 + oysters in 2018 was 0.40%.

Bottom Water DO: Continuous Autonomous Monitoring

The greatest DO depletion and daily O_2 excursion occurred in late summer when temperature-dependent oxygen solubility was low and oxygen demand by marine communities was high; DO availability increased towards fall as waters cooled and fall storms increased water column mixing. Temperature profiles (not shown) indicated weak water column stratification during July and August. We observed consistent overlap between time series records of surface and bottom water DO concentrations for the duration of sonde deployment (Fig. 2). Here, the 2018 sonde data is shown because it provides the longest uninterrupted DO time series and is consistent with 2016 and 2017 results. During August, bottom water (0.3 m from bottom; ~ 1.8 m total depth) time series typically showed greater DO variability compared to surface waters (0.5 m from surface; ~ 3.5 m total depth), with daily O_2 excursions up to ~ 6 mg L^{-1} (daylight O_2 above atmospheric equilibration levels and nighttime O_2 depletion). DO concentrations above Commonwealth MA water quality standards (> 6 mg L^{-1}) accounted for 68% and 63% of the 2018 surface and bottom records, respectively. However, DO concentrations less than 6 mg L^{-1} occurred during the warmest period from early August to mid-September when SOD was greatest and bottom water re-aeration was periodically limited by low water column mixing. Despite direct contact with the atmosphere, O_2 consumption in surface waters exceeded rates of re-aeration, resulting in DO declines to less than 4 mg L^{-1} during late summer.

Water Column N

Stream inputs of DIN to Lonnie's Pond were highest in May and decreased through the summer. Interannual differences in rainfall and stream-related inputs resulted in a two-fold increase from 0.1 to 0.2 mg L^{-1} in average monthly

Table 1 Dates of oyster deployment and removal, and dry tissue weight (DTW) densities relative to the number of bags deployed (g DTW bag^{-1}) and pond surface area over which floating bags were deployed (g DTW m^{-2})

Year; cohort		Deployment period	Stocking density (oysters bag^{-1})	Shell height (mm)		Stocking density (g DTW bag^{-1})		Oyster growth (g DTW bag^{-1} day^{-1})	Deployment area (m^2)	Deployment density (g DTW m^{-2} deployment area)		Oyster growth (g DTW m^{-2} day^{-1})
				Initial	Final	Initial	Final			Initial	Final	
2016	0 +	6/22–12/14	250	32.0 ± 3.5	74.3 ± 10.1	9.2 ± 1.9	272.1 ± 10.5	1.5 ± 0.8	892	8.2 ± 1.8	244.1 ± 9.6	1.4 ± 0.7
	1 +		250	62.9 ± 7.4	94.0 ± 13.1	122.3 ± 12.9	461.8 ± 25.4	1.9 ± 1.7		109.7 ± 12.4	414.3 ± 24.0	1.7 ± 1.6
2017	0 +	5/12–12/20	6000–800[a]	2–3[b]	53.0[b]	1.2 ± 0.9	295.3 ± 8.9	1.3 ± 0.6	756	1.0 ± 0.7	391.1 ± 18.8	1.8 ± 1.1
	1 +	5/4–11/16	260	50.8[b]	89.5[b]	152.8 ± 16.5	441.8 ± 25.0	1.7 ± 1.4		205.6 ± 18.4	564.9 ± 26.0	2.1 ± 1.4
2018	0 +	5/19–12/17	770[a]	2–3[b]	60.0[b]	1.1 ± 0.8	208.3 ± 11.2	1.0 ± 0.8	1134	1.5 ± 1.0	280.3 ± 13.0	1.3 ± 0.9
	1 +	4/20–11/10	285	53.0[b]	86.0[b]	104.7 ± 8.6	263.2 ± 13.7	0.8 ± 0.8		140.9 ± 10.7	354.2 ± 15.9	1.1 ± 0.8

[a]0 + year class 2017 and 2018 oysters were first deployed as 2–3 mm seed in modified floating spat bags, and then redeployed in 6-mm mesh bag
[b]Town of Orleans Water Quality and Wastewater Planning (2018)

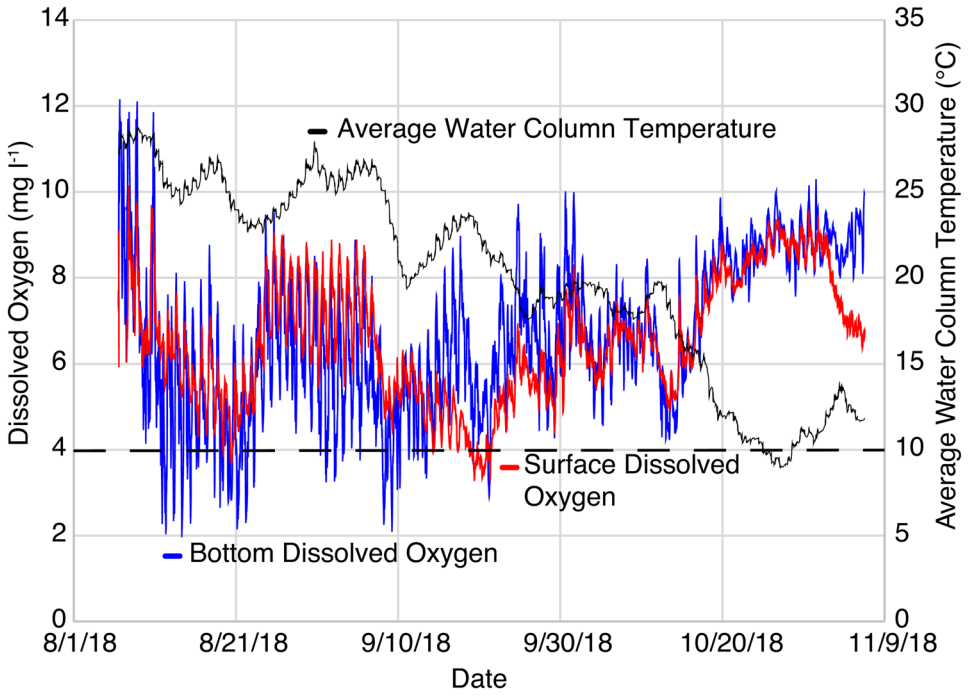

Fig. 2 August to November 2018 time series DO concentrations from surface and bottom water column moored sondes. The bottom sonde was deployed directly below the floating oyster bags (most biodeposits settle directly below source bags) to capture impacts of increased deposition on DO. Periodic low DO events (< 4 mg L^{-1}) occurred when temperatures were above 20 °C; however, these events were typically brief (< 24 h) and DO was typically above 2 mg L^{-1}

DIN levels due to the loading variation from 2017 to 2018; in addition, the major fraction of NH_4^+ and NO_x^- in DIN shifted from NH_4^+ in 2017 to NO_x^- in 2018. In contrast to stream loads, water column NO_x^- was consistently the smallest fraction of DIN and TN pools; NO_x^- concentrations were typically ~ 3.3 µM lower compared to NH_4^+. Monthly NO_x^- and NH_4^+ concentrations showed a clear temporal trend with maximum levels in October (Fig. 3). October NO_x^- concentrations were ~ 16 times higher compared to June; therefore, the diffusional supply of water column NO_x^- (potentially available to denitrifying bacteria) was highest in October and lowest in June. Bottom

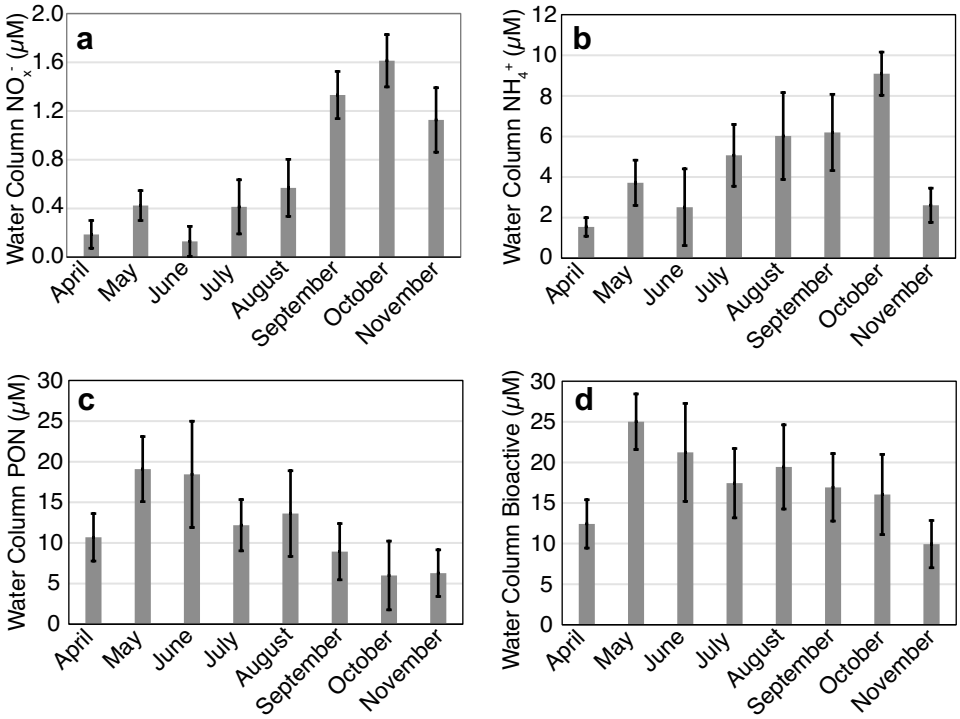

Fig. 3 Mean monthly water column combined nitrate (NO_x^-; **a**), ammonium (NH_4^+; **b**), particulate organic N (PON; **c**), and bioactive N ($NO_x^- + NH_4^+ +$ PON; **d**) concentrations from April–November samplings of water quality sites distributed throughout the pond (2016–2018). Vertical error bars represent 1 standard deviation. Water column NO_x^- can diffuse from the water column into the sediment for use by denitrifying bacteria via direct denitrification. Note the different *y*-axis limits

Table 2 Comparison of mean ± SD sediment oxygen demand (SOD) and flux of dissolved inorganic nutrients (mmol O_2, N, or P m^{-2} day^{-1}) from treated (within biodeposit area) and control areas (outside biodeposit area), collected in Lonnie's Pond during summer, fall, and spring* of 2016, 2017, and 2018. A positive value for nutrients indicates an average outward flux from the sediments, and a negative value an average uptake by the sediment from the water column

	Year 1 (2016)		Year 2 (2017)		Year 3 (2018)	
	Treated	Control	Treated	Control	Treated	Control
			SOD (oxygen uptake)			
Summer	161.06 ± 111.09	99.77 ± 36.83	104.10 ± 42.68	68.11 ± 17.23	151.34 ± 90.53	76.61 ± 20.86
Fall	71.08 ± 39.58	49.98 ± 26.51	52.34 ± 31.11	36.73 ± 18.25	59.73 ± 12.25	60.09 ± 33.20
Spring	60.02 ± 22.22	33.36 ± 9.80	-	-	53.92 ± 18.58	61.24 ± 29.57
			PO_4^{3-}			
Summer	2.41 ± 1.84	0.68 ± 0.36	1.14 ± 1.10	0.40 ± 0.45	0.46 ± 0.47	0.70 ± 0.16
Fall	−0.19 ± 0.13	−0.04 ± 0.20	0.01 ± 0.18	0.10 ± 0.12	0.69 ± 1.06	0.17 ± 0.23
Spring	−0.01 ± 0.06	0.00 ± 0.08	-	-	−0.05 ± 0.10	−0.02 ± 0.13
			NH_4^+			
Summer	18.26 ± 9.41	4.88 ± 2.59	7.45 ± 4.40	4.78 ± 2.41	12.49 ± 6.19	7.33 ± 4.02
Fall	3.06 ± 3.23	0.32 ± 2.65	3.42 ± 1.99	0.61 ± 0.23	3.31 ± 1.42	1.93 ± 1.50
Spring	0.59 ± 0.73	−0.18 ± 0.09	-	-	1.04 ± 0.71	1.18 ± 1.16
			NO_x^-			
Summer	0.20 ± 0.21	0.08 ± 0.09	0.08 ± 0.14	0.23 ± 0.20	1.35 ± 1.88	0.75 ± 0.43
Fall	−0.33 ± 0.16)	0.06 ± 0.54	−0.14 ± 0.16	−0.10 ± 0.06	−0.10 ± 0.14	−0.12 ± 0.07
Spring	−0.11 ± 0.06	−0.09 ± 0.02	-	-	−0.02 ± 0.01	−0.04 ± 0.03

*A spring sediment incubation was not conducted during year 2 (2017)

water NH_4^+ concentrations in July, August, and September (~ 5–6 µM) represented summer highs likely because of higher rates of NH_4^+ production during the warmest months. Elevated levels of water column NO_x^- + NH_4^+ in October, which could not be explained by stream input (DIN loading decreased ~ 80% from May to Oct/Sep), were likely the result of internal processes, such as regeneration of deposited organic matter and reduced primary productivity in response to cooling waters and decreasing light availability. PON concentration, like DIN loading, was highest in May and decreased towards fall (Fig. 3), suggesting that stream inputs of DIN to the pond were rapidly taken up by phytoplankton and converted from dissolved N to particulate N in phytoplankton biomass.

Sediment Oxygen and Nutrient Fluxes

The highest SOD flux rates of each core sampling event were measured in treated cores, with the highest overall being in summer 2016 and 2018 (Table 2). The lower summer 2017 SOD rates corresponded with observations of minimal redox potential discontinuity (RPD; i.e., sediment color change from brown to grey/black) depth and sulfidic surficial sediments and the absence of benthic animals. The effect of the RPD depth can also be seen in the lower NH_4^+ and NO_x^- flux rates in summer 2017 compared to summer 2016 and 2018; N fluxes are described below. In addition, there was a significant interaction effect between treatment and season for SOD rates ($n = 117$) where summer treated cores had higher SOD compared to control cores and fall treated and control cores $F(1, 105) = 5.33$, $p = 0.023$ (Table 3). This interactive effect is the result of greater rates of bacterial activity during the warm summer months when there is higher organic matter availability in the biodeposit area.

On average, there was net inorganic phosphorus release from the sediments to the water column in summer. However, we found a significant interaction between treatment, season, and year (3-way ANOVA, $F(2, 89) = 3.98$, $p = 0.0221$; Table 3). The effect of treatment and season differed by year because of the high mean summer treated

Table 3 *F*-values of 3-way ANOVA for the main and interactive effects of treatment (biodeposit affected and background), season (summer and fall), and year (2016, 2017, and 2018) on sediment oxygen demand (SOD), and ortho-phosphate (PO_4^{3-}), ammonium (NH_4^+), and combined nitrate (NO_x^-) sediment flux rates

Variable	Treatment (T)	Season (S)	Year (Y)	T × S	T × Y	S × Y	T × S × Y
SOD	**12.62**	**32.03**	**3.88**	**5.33**	0.27	0.73	0.81
PO_4^{3-}	**5.43**	**21.90**	0.97	3.18	0.98	**5.01**	**3.98**
NH_4^+	**30.93**	**70.80**	**4.33**	**7.96**	**3.55**	**4.2**	**3.41**
NO_x^-	0.08	**17.84**	**5.40**	1.30	1.14	**5.41**	0.78

Boldface *p* indicates significance at $\alpha = 0.05$

PO_4^{3-} flux measured in 2016 (Table 2). PO_4^{3-} efflux from treated cores collected during summer months was significantly greater compared to both fall treatments and summer control cores. Also, PO_4^{3-} efflux measured in August 2016 was significantly greater compared to October 2016 and summer and fall of 2017 and 2018. PO_4^{3-} efflux from treated and control sediments occurred during periods of low bottom water DO concentrations (~ 1 mg L^{-1} in 2016) when RPD was very shallow/non-existent.

On average, NH_4^+ fluxes to bottom water in the biodeposit area was significantly greater than from control areas in all years and seasons; however, there was a significant interaction between treatment, season, and year (3-way ANOVA, $F(2, 103) = 3.41$, $p = 0.0367$; Table 3). The interaction stems from the greater release in summer versus fall in all years and both treatments where summer months had higher temperatures and biodeposition rates are greatest. However, NH_4^+ efflux from treated cores collected during summer months in 2016 and 2018 for all cores was significantly greater than 2017 summer rates.

Uptake and efflux of NO_x^- across the sediment surface varied seasonally with NO_x^- uptake during fall and spring when SOD is also lowest and net efflux during the warmer summer months (Table 2). Only August 2017 showed summer NO_x^- uptake. We found a significant interaction between season and year (3-way ANOVA, $F(2, 97) = 5.41$, $p = 0.0059$; Table 3). The average NO_x^- efflux from sediments receiving biodeposits in summer 2018 was about 6 times greater compared to 2016 and 11 to 33 times greater compared to 2017 (Table 2). This suggests that NH_4^+ production and a thicker oxidized surface layer (see below) favored nitrification. However, the treatment effect for NO_x^- efflux was not significant during any year. NO_x^- fluxes were generally similar in summer and fall both within and between years 2016 and 2017.

Small-scale sediment heterogeneity was observed by divers during all 3 years of the study, including differences in coloration of surficial sediments ranging from light brown to grey/black, and the presence of faunal burrows and burrow dwelling macrofauna (e.g., amphipods and polychaetes). Redox potential discontinuity (RPD) depth in individual cores varied between flux dates and core location on a single flux date. RPD depths tended to be shallower during periods of high organic matter loading and low (< 6 mg L^{-1}) bottom water DO. Treated cores (i.e., biodeposit affected) collected in summer 2016 and 2017 were characterized by shallow or negligible RPD depths. September 2017 sediments were notable because nearly all treated cores had large surficial patches of black sulfidic mud. Sulfidic sediments persisted into October 2017, but to a lesser extent. Compared to previous summer fluxes, all July 2018 treated cores had a thicker oxidized surface layer. However, the oxidized surface layer gradually thinned from July to October 2018 with only a thin oxidized layer in several treated cores collected in October. April treated and control cores typically had a light brown uniform oxidized surface. In addition, it is important to note that shallow RPD depths were not limited to treated cores. Some August 2017 and July 2018 control cores also had patches of gray/black in the surficial sediments.

Nitrogen Deposition and Cycling in Sediments

Monthly N deposition rates (biodeposition + background deposition) associated with individual core locations were modeled for summer and fall 2017 and 2018 (Labrie et al. 2022); mass balance plots (Fig. 4, x-axis) represent four of these six dates. June 2017 data are not shown since the experiment was designed to capture summer, fall, and following early spring conditions; July 2017 is not shown since no sediment flux data were collected during that period; and September 2017 and October 2018 fluxes (not shown) were excluded because sulfidic surface sediments dominated the treated area. More specifically, September 2017 treated cores had the highest N deposition rates (563.7 mmol N m^{-2} $month^{-1}$). Minimum N deposition rates (control) ranged from 40.5 in October 2018 to 111.7 mmol N m^{-2} $month^{-1}$ in July 2018. In contrast, 2018 deposition rates in treated cores averaged 350.0 ± 191.7 mmol N m^{-2} $month^{-1}$ in July and 220.9 ± 104.7 mmol N m^{-2} $month^{-1}$ in October, whereas control areas averaged 191.9 ± 49.5 mmol N m^{-2} $month^{-1}$ in July and 52.8 ± 16.1 mmol N m^{-2} $month^{-1}$ in October. The decrease in background deposition rates from July to October reflected seasonality of water column PON concentrations, with July having the highest deposition rate followed by June 2017 (148.7 ± 16.1 mmol N m^{-2} $month^{-1}$). The low oyster biomass in June 2017 and low growth rates in 2018 produced low deposition rates (primarily biodeposition N). For these reasons, June 2017 and July 2018 deposition rates did not differ between treated and control areas (June 2017: $t = 1.95$, $df = 14$, $p = 0.072$; July 2018: $t = 1.96$, $df = 14$, $p = 0.071$). In contrast, the deposition rates were higher in treated and control cores for all other fluxes dates (August 2017: $t = 2.54$, $df = 14$, $p = 0.024$; September 2017: $t = 4.59$, $df = 14$, $p = 0.0004$; October 2017: $t = 4.68$, $df = 14$, $p = 0.0004$; and October 2018: $t = 3.85$, $df = 14$, $p = 0.002$).

Monthly denitrification rates increased linearly with N deposition (biodeposition + background deposition) in June 2017, July 2018, and October 2017 (left *y*-axis; Fig. 4). Of the 3 months, June showed the closest relationship between N deposition and denitrification, explaining 80% of the variation. On average, 8% ± 5% of N deposition ended up denitrified, consistent with the slope of the linear regression (10.8%). June 2017 also coincided with the lowest measured water column NO_x^- levels. In October and July, denitrification also showed a positive linear increase with

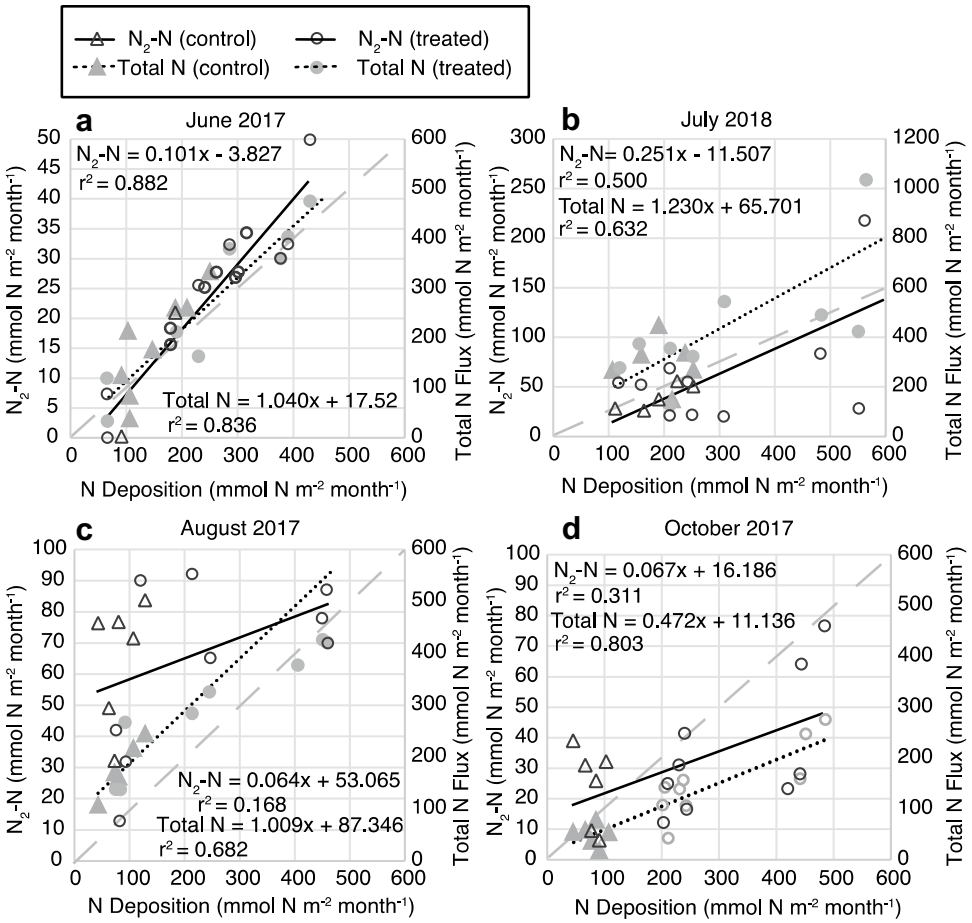

Fig. 4 Mass balance of monthly predicted deposited N (N; biodeposition + background) and measured flux of N_2-N (left axes), and total N (NH_4^+, NO_x^-, N_2-N, plus dissolved organic N; right axes) flux to the water column from the sediments in June 2017 (**a**), July 2018 (**b**), August 2017 (**c**), and October 2017 (**d**). Data points represent individual cores; triangles (open and filled) are control cores collected outside of the biodeposit area; and circles (open and filled) are treated cores collected within the biodeposit area. Deposited N is based on a biodeposit model (Labrie et al. 2022) specific to each core location. Linear regression of deposited N and N_2-N flux (open triangles/circles) and deposited N and total N (filled triangles/circles) is shown. N_2-N increased linearly with N deposition in June (95% CI 0.074 to 0.146, $n = 9$), July (95% CI 0.107 to 0.394, $n = 16$), and October (95% CI 0.008 to 0.129, $n = 15$). Total N release increased linearly with N deposition in June (95% CI 0.776 to 1.303, $n = 16$), July (95% CI 0.692 to 1.768, $n = 16$), August (95% CI 0.575 to 1.44, $n = 14$), and October (0.332 to 0.612, $n = 15$). Gray dashed lines represent 1:1 lines corresponding to total N flux on the right y-axis

N deposition, but the proportion of variance in N_2-N was greater than in June 2017 as seen in the lower coefficients of determination ($r^2 = 0.31$ and 0.50 for October 2017 and July 2018, respectively; left *y*-axis; Fig. 4). The July 2018 results showed three times higher mass of N deposition denitrified (21% ± 12% of N deposition) than in June 2017, suggesting that the amount of N deposited and the environmental conditions in July were slightly more conducive to denitrification compared to June. The August 2017 flux did not yield a significant linear regression due to a large range of denitrification rates under low deposition rates, around 100 mmol N m^{-2} $month^{-1}$ (left *y*-axis; Fig. 4). Denitrification accounted for 34% ± 21% (treated) and 88% ± 47% (control) of total deposition. Only a weak positive relationship was found between N deposition and denitrification in September 2017 ($r^2 = 0.079$) or October 2018 ($r^2 = 0.026$).

Monthly total N (dissolved organic and inorganic N, and N_2-N) efflux from sediments was positively correlated with N deposition in June 2017, July 2018, August 2017, October 2017 (Fig. 4, right axis; see figure and caption for regression statistics), September 2017 ($r^2 = 0.472$, slope = 0.278, 95% CI 0.071 to 0.485, $n = 12$), and October 2018 ($r^2 = 0.423$, slope = 0.244, 95% CI 0.043 to 0.445, $n = 12$). During the summer months (June, July, and August), the slopes from linear regressions of deposition versus regeneration remained above the 1:1 line (i.e., slope ≥ 1). Similarly in fall (September 2017, October 2018), linear regressions also had slopes

less than one. Furthermore, we calculated monthly rates of total N regeneration as a percent of monthly mass of N deposition to the sediment surface. This provides an estimate of the portion of total N deposition that was regenerated in the control vs. treated areas. Percentages did not differ between treated and control areas for June ($t = -0.641$, df = 14, $p = 0.532$), August ($t = -1.147$, df = 13, $p = 0.272$), and October 2017 ($t = -1.499$, df = 14, $p = 0.156$) and July 2018 ($t = -0.416$, df = 14, $p = 0.684$), indicating that regeneration was directly linked to deposition, and that the deposited organic matter is likely similarly labile between the two areas, which is reasonable since both are phytoplankton based. Treated and control data were thus pooled to examine the overall relationship of deposition to regeneration. The results suggest that an amount of N equivalent to the deposited N is remineralized rapidly, and percentages > 100% indicated some regeneration of residual sediment N from prior deposition. The percent regeneration of deposited organic N during summer months ranged from 107 to 186% and decreased to 55% ± 28% in October 2017. The proportion of total N regenerated to N deposited was lower in treated cores than control cores in September 2017 (treated = 51%, control = 195%) and October 2018 (treated = 59%, control = 130%). The lower regeneration in fall is consistent with the high rates of regeneration the following spring prior to the onset of biodeposition from spring oyster deployment.

Water column C:N molar ratios (Table 4) averaged 7.2 ± 1.0 (POC:1PON) for the combined flux dates. Molar ratios for the sediment–water column exchange rates (C:N and N:P) were calculated for each core where C:N was determined as the ratio of the rates of SOD and total N efflux, using a 1: 1 ratio of CO_2:O_2 and the empirical molar N:P ratio determined from the ratio of total N efflux rate to PO_4^{3-} efflux rate (Table 4). Measured flux rates in treated and control cores did not yield significantly different C:N and N:P molar ratios ($p > 0.05$); therefore, treated and control ratios were pooled to examine the overall relationship. Averaging sediment flux C:N and N:P ratios over the 3 project years resulted in ratios of 9.9 ± 2.4 C:1 N and 17.7 ± 8.6 N:1P.

Annual N Removed by Aquaculture: Denitrification and Assimilation/Harvest

Total annual N biodeposition was highest in 2017 (Table 6). 2018 had the largest initial oyster population; however, N biodeposition (9.2 g N m^{-2}) was only ~ 40% of that in 2017 (23.3 g N m^{-2}) and ~ 75% of that in 2016 (12.3 g N m^{-2}). N biodeposition rates peaked in early September of all 3 years. September DTWs were 248 g DTW m^{-2}, 420 g DTW m^{-2}, and 226 g DTW m^{-2} in 2016, 2017, and 2018, respectively.

Enhancement of microbial denitrification within the biodeposit area resulted in 5.0–12.1 kg N (3.778 to 4.445 g m^{-2}) removal per year over control areas. We observed significant denitrification enhancement on 80% of the flux dates; only August and September 2017 did not have significant denitrification enhancement (Table 5). In August 2017, we found NO_x^- uptake in six of the eight treated cores and one of the six control cores (pooled average = −0.06 ± 0.03 mmol N m^{-2} day^{-1}); the percentage of total denitrification from direct denitrification (assuming measured NO_x^- uptake is equivalent to direct denitrification) averaged 2.6 ± 1.2% in August 2017 treated cores. Nitrate uptake was observed during fall of all 3 years. The percentage of total denitrification from direct denitrification in October 2016, 2017, and 2018 could be as high as 13.4% ± 7.6%, 11.9 ± 4.3%, and 32.4 ± 22.6%, respectively. Finally, early spring denitrification rates in sediments receiving biodeposits (pooled average year 1 and year 3 = 2.29 ± 1.51 mmol m^{-2} day^{-1}) were nearly triple control

Table 4 Mean ± SD C:N molar ratios of water column particulate organic carbon (POC) and N (PON) and sediment flux of C and N. Molar ratios using individual core sediment oxygen demand and total N efflux (NH_4^+, NO_x^-, N_2-N, and dissolved organic N). We assumed that the molar ratio of CO_2:O_2 during respiration was 1:1 on the condition that the reduced end-products of anaerobic respiration were oxidized by O_2, in the surficial sediments

Project year	Date	Water column C:N	Biodeposit C:N	Sediment flux C:N	Sediment flux N:P
Year 1	Aug '16	5.9 ± 0.3	ND	7.4 ± 1.9	12.9 ± 5.4
	Oct '16	8.6 ± 0.2	9.3 ± 0.4	8.2 ± 2.3	30.9
	Apr '17	9.1 ± 2.5	ND	12.7 ± 4.6	13.0 ± 7.5
Year 2	Jun '17	5.9 ± 0.2	ND	11.7 ± 2.3	7.7 ± 5.2
	Aug '17	6.4 ± 0.7	6.6 ± 0.04	8.6 ± 2.7	13.0 ± 7.1
	Sep '17	7.3 ± 0.7	6.6 ± 0.03	11.0 ± 2.2	14.4 ± 7.1
	Oct '17	6.9 ± 0.7	7.5 ± 0.5	10.0 ± 2.8	15.4 ± 5.8
Year 3	Jul '18	6.4 ± 1.1	ND	8.0 ± 1.2	18.4 ± 10.0
	Oct '18	7.2 ± 0.6	ND	10.3 ± 2.8	14.9 ± 13.1
	Apr '19	7.9 ± 0.8	ND	11.4 ± 2.2	36.7 ± 15.6

Table 5 Incubation temperature (°C), denitrification (mmol N_2-N m^{-2} day^{-1}), and nitrogen (N) efflux (mmol N m^{-2} day^{-1}) measured in intact sediment cores collected inside vs. outside biodeposit areas (treated vs. control). Difference between the two rates represents denitrification enhancement in biodeposit-affected sediments above background rates. The percentage of the total N denitrified is the portion of measured total N efflux that was N_2-N. Nitrogen rates are averages ± SD

Project year	Date	Temperature (°C)	Denitrification (mmol N_2-N m^{-2} day^{-1})						N efflux (mmol N m^{-2} day^{-1})		Percent N efflux denitrified (%)
			Treated	Control	Enhancement	t Stat	df	*p*	Treated	Control	
Year 1	Aug '16	27.3	3.0 ± 1.1	1.7 ± 0.3	**1.2 (69%)**	1.88	7	0.051	22.4 ± 12.0	8.5 ± 2.3	21 ± 12
	Oct '16	16.2	2.8 ± 1.1	1.7 ± 0.7	**1.1 (62%)**	1.69	8	0.064	6.6 ± 2.6	3.7 ± 0.7	31 ± 14
	Apr '17	10.5	2.7 ± 1.7	0.9 ± 0.3	**1.8 (202%)**	2.74	11	0.010	2.5 ± 2.5	1.0 ± 0.3	70 ± 32
Year 2	Jun '17	22.2	1.3 ± 0.4	0.3 ± 0.4	**1.0 (343%)**	4.14	11	0.001	9.0 ± 5.2	6.2 ± 3.3	12 ± 8
	Aug '17	24.1	2.1 ± 0.9	1.6 ± 0.8	0.5 (29%)	0.91	11	0.192	12.2 ± 7.1	7.1 ± 3.1	18 ± 9
	Sep '17	22.9	0.7 ± 0.9	0.2 ± 0.1	0.5 (236%)	1.19	8	0.134	8.6 ± 5.1	6.4 ± 2.0	7 ± 11
	Oct '17	17.7	1.5 ± 0.9	0.7 ± 0.4	**0.8 (107%)**	2.06	13	0.030	4.8 ± 2.5	1.6 ± 0.7	29 ± 15
Year 3	Jul '18	23.7	3.3 ± 2.5	1.2 ± 0.4	**2.2 (186%)**	2.24	12	0.022	16.6 ± 10.2	9.9 ± 3.3	14 ± 7
	Oct '18	18.8	0.5 ± 0.3	0.2 ± 0.3	**0.4 (196%)**	2.25	9	0.025	4.4 ± 2.4	2.2 ± 1.4	9 ± 4
	Apr '19	12.0	1.8 ± 1.2	0.3 ± 0.5	**1.4 (354%)**	2.74	12	0.009	2.0 ± 1.4	3.3 ± 1.4	37 ± 19

Boldface type indicates significance at $\alpha = 0.07$, which we chose given the heterogeneity of the biogeochemical fluxes

rates (pooled average year 1 and year 3 = 0.84 ± 0.37 mmol m^{-2} day^{-1}), but NO_x^- uptake was similar between treated and control cores (the pooled average for all cores year 1 and year 2 was − 0.06 ± 0.03 mmol m^{-2} day^{-1}). During spring, direct denitrification contributed more to total denitrification in control areas than treated, and in year 1, the percent direct denitrification of total denitrification (treated and control) was more than double the percent direct denitrification of total denitrification in year 3. Looking at direct denitrification rates as a percent of total denitrification in year 1, the treated percentage was 3.3 ± 1.7% and the control percentage was 10.3 ± 3.8%, while in year 3, the treated was 1.7 ± 1.6% and control was 4.8 ± 3.2%.

The mass of N removed through harvest (i.e., oyster removal at end of the growing season) increased from 2016 to 2018, coinciding with increasing level of oyster deployment (Table 6). N assimilation normalized to deployment duration shows that oysters assimilated 148.3, 141.7, and 174.2 g N day^{-1} overall in 2016, 2017, and 2018, respectively. In 2016, the 1 + cohort contributed 76% of the total assimilated N from both cohorts, while in 2017 and 2018, 0 + and 1 + cohorts each contributed ~ 50%; the relative contribution reflected the proportion of 0 + and 1 + oysters deployed in each year. However, in 2018, 1 + oysters removed 3.3 more kg N compared to 0 + oysters because percent N content of 1 + oysters was higher compared to all other years and cohorts.

Annual N Mass Balance

To examine how N dynamics are altered by floating oyster aquaculture, a mass balance of N cycling was constructed for the two water column/sediment systems in which measurements were made: (1) floating oyster aquaculture areas and (2) natural areas without aquaculture (Fig. 5). Sediment–water column exchange (flux) rates were expressed as g N g^{-1} DTW

Table 6 Annual N removal budget for the 3 study years showing contributions from enhanced denitrification and oyster harvest

	Year 1 (2016)	Year 2 (2017)	Year 3 (2018)
Time deployed (days)	175	230	241
Annual biodeposition of N (kg N)	19.1	27.0	25.0
Enhanced annual denitrification (mmol N m^{-2})	308.7	269.7*	317.4
Enhanced annual denitrification (g N m^{-2})	4.3	3.8	4.4
Normalized to biodeposition (mmol N kg^{-1} N m^{-2})	16.1	10.0	12.7
Biodeposit area (m^2)	1574.6	1334.5	2717.4
Total annual enhanced denitrification (kg N)	6.8	5.0	12.1
Net annual N removed by harvest (kg N)	25.9	27.2	36.2
Enhanced denitrification as a percent of N mass removed by harvest (%)	26.3	18.5	33.4

*Year 2 (2017) spring carryover additions were estimated from year 1 and year 3 April enhanced denitrification measurements; the year 2 enhanced denitrification estimate accounted for differences in biodeposition between years

m^{-2} and g N m^{-2} for treated and control areas, respectively. Oyster N assimilation, N biodeposition, and dissolved inorganic N and N_2-N sediment fluxes were determined through direct measurements. Settling of background N particles was estimated from average daily water column PON concentrations assessed through linear interpolation between water quality sampling events and a turnover of 15.5% per day (Lohrenz et al. 1987). Oyster filtration rate used published studies on the volume of water cleared of particles by oysters per unit time (Comeau, 2013), and average daily water column PON, to get the mass of N filtered from the water column per day. Comeau (2013) determined a clearance rate of 4.34 l h^{-1} standardized to 1-g DTW suspended oysters based on laboratory measurements on single oysters. Biodeposition rates standardized to a 1-g DTW oyster measured in situ from both single oysters and whole oyster bags in Lonnie's Pond suggest that single oyster rates were on average 10 times higher than rates measured from whole oyster bags under comparable environmental conditions. Biodeposit traps deployed in Lonnie's Pond during summer and fall measuring biodeposition rates (standardized to a 1-g DTW oyster) of individual oysters and whole oyster bags had an average (±SD) biodeposition rate of 158.8 ± 88.3 mg dry wt DTW^{-1} day^{-1} and 16.4 ± 6.6 mg dry wt DTW^{-1} day^{-1}, respectively. The observed rate difference appears to result from the effects of crowding and competition between oysters for food particles in a floating bag versus when individually deployed. To account for this difference, we multiplied the Comeau (2013) clearance rate by a correction factor (0.10) to determine the volume of water cleared of N particles per day by the full oyster deployment. We estimated N excretion using an average rate of 6.0 µmol NH_4^+ g^{-1} h^{-1} (Magni et al. 2000) for 11 species of bivalve mollusc, which agrees with data from Srna and Baggaley (1976) for eastern oysters. Like clearance rate (i.e., filtration), the excretion rate was multiplied by 0.10 assuming a proportional decrease in excreted N with decreased N filtration. Last, burial rates of PON from biodeposition and background settling were estimated by applying a sediment accretion rate typical of Cape Cod embayments and measurements of N content in the upper 2 cm of sediment in treated and control areas. We used an average accretion rate calculated from annual accretion rate measurements in nearby Little Pond, Falmouth, based on

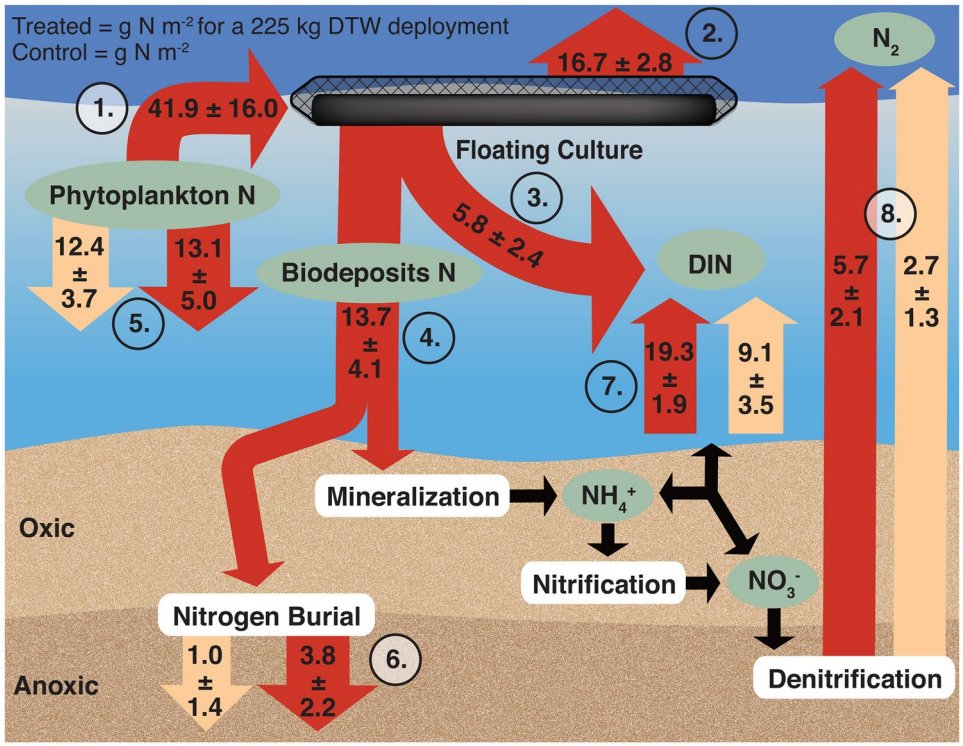

Fig. 5 Mass balance comparison of nitrogen (N) cycling in areas receiving biodeposits from floating oyster aquaculture (red arrows) vs. control/natural areas (beige arrows) without floating oyster aquaculture. All arrows represent a 3-year (2016–2018) average of N fluxes (mean ± SD) over the oyster growing season. Treated fluxes were normalized by the season average of dry tissue weight (DTW) biomass and biodeposit area for each project year, expressed as g N m^{-2} for a 225 kg DTW deployment. Control fluxes were normalized by the biodeposit area for each project year, expressed as g N $m^{-.2}$. Transformations are as follows: (1) N removed from the water column via oyster filtration, (2) net N assimilated into oyster biomass over the growing season, (3) oyster excretion, (4) biodeposition, (5) background N deposition to the biodeposit area, (6) burial, (7) dissolved inorganic N efflux from mineralization and nitrification, (8) denitrification

Pb^{210} (3 mm $year^{-1}$); accretion rates were generally comparable to rates of sea level rise.

Oyster physiological processes vary seasonally with seasonal changes in temperature, food availability, and oyster biomass. Oysters directly contributed to permanent N removal through filtration and assimilation by incorporating 40% of ingested PON into oyster biomass (Fig. 5). In addition, oyster filtration and egestion transferred large amounts of PON from the water column to the sediments; this biodeposition accounted for 51% of total N deposition. The main pathways of N removal from active cycling associated with floating oyster aquaculture were assimilation/removal (64%), enhanced denitrification (22%), and burial (14%).

Discussion

Effect of Oyster Aquaculture on N Cycling

Comparison of the N mass balance of a floating oyster aquaculture system with the nearby estuarine area not affected by oyster aquaculture revealed that oysters have a significant effect on N and C cycling in their local environment. Results also show that significant N can be removed through their growth and subsequent removal from the system, and by their influence on sediment denitrification through their biodeposits (Fig. 5). Before floating oyster aquaculture was established in the relatively shallow waters of Lonnie's Pond, deposition of organic N and C (primarily phytoplankton) to the sediment via zooplankton grazing and direct settling determined sediment respiration rates as modified by temperature. After aquaculture was established, oyster filtration/biodeposition more than doubled the mass of N reaching the sediments. Nitrogen mass balances within the floating oyster aquaculture system indicate that ~ 54% of PON filtered from the water column was incorporated into oyster biomass or excreted as dissolved N. Of the 54% PON that was assimilated, 74% was incorporated by the oysters into biomass. The amount of biodeposits was less well constrained, ranging from 33 to 46% (Fig. 5). A study by Songsangjinda et al. (2000) using floating bag oyster aquaculture found comparable apportioning with only a slightly higher value of 44% biodeposits. In addition, our percent biodeposit apportionment was lower than that reported by Newell and Jordan (1983; 50% filtered N released as biodeposit N) for bottom raised oysters, but this difference was expected given the physiological differences between surface and bottom raised oysters (Comeau, 2013).

A clear response in the cycling of sediment organic matter was found using measurements of oxygen consumption and NH_4^+ efflux within the biodeposit area (treated) compared to the control area, especially during the summer months (Table 2). The results suggest that biodeposits enhanced remineralization of organic C and N in surficial sediments, and more importantly, that denitrification was enhanced where biodeposition was occurring (Table 5; Fig. 5). The mass balance of N cycling in a floating oyster aquaculture system and an estuarine system not affected by oyster aquaculture indicates that, on an annual basis, the presence of oysters significantly increases respiration and denitrification in sediments. Oyster biodeposit production thus accelerates N cycling within the biodeposit area, which in turn enhances N removal from the estuarine ecosystem.

Seasonality of Biodeposit Remineralization

Tracking of sediment C and N remineralization and deposition indicated that sediments tend to remineralize most fresh deposits and even some stored deposits in summer, and then store organic matter in fall into the following spring. Efflux of remineralized N was well predicted based on biodeposition and an empirical model (Labrie et al. 2022). In addition, average C:N and N:P ratios of nutrient regeneration of all cores (9.9C:1 N and 17.7 N:1P) were comparable to the Redfield ratios for marine phytoplankton (i.e., 6.6C:N and 16.1 N:P). Mass balance regressions of predicted N deposition and sediment N efflux suggested rapid regeneration of organic N deposited during summer months as seen in linear regressions (Fig. 4, slopes above 1.0), with data above the 1:1 lines indicating net organic matter regeneration rather than storage. Rapid cycling of summer biodeposits was also evidenced by 3-way ANOVA results, where SOD and nutrient fluxes were significantly greater during summer months when phytoplankton biomass was high as a result of warm temperatures and light availability. The result was maximum oyster filtration and biodeposition and high background deposition rates. Particulate organic N, an indicator of food availability, peaked between 15 and 20 µmols L^{-1} during May and June, with concentrations trending downward towards fall (Fig. 3). The slope of the October 2017 linear regression of N deposition and N efflux indicated a ~ 50% lower regeneration rate per unit deposition compared to June 2017 and July 2018, suggesting a larger fraction of deposited N was being stored in the sediments in fall. These results supported our hypothesis that a seasonal lag exists between fall deposition of organic matter and the regeneration of nutrients and denitrification in early spring. We suggest that cooler fall temperatures lead to lower sediment flux rates and greater accumulation of labile organic matter in subsurface sediments. Organic matter respiration is a function of temperature (Jorgensen, 1975); therefore, decreasing temperatures between fall and winter lead to a concomitant decrease in microbial activity, which favors accumulation and storage

of deposited N in sediments below the thin surficial oxic layer (Rudnick and Oviatt 1986). Enhanced denitrification in early spring increased annual N removal in oyster areas by 1.8 kg and 3.2 kg above previous summer and fall enhancement, yielding a 42% and 37% increase in the total annual N removed via enhanced denitrification in 2016 and 2018, respectively. Based on these results, future assessments of oyster aquaculture enhanced denitrification should include measurements the following early spring to capture the effects of overwintered biodeposits. Biodeposits accumulate during fall and may persist for months to 1 + years. Thus, the period of enhanced denitrification appears to extend beyond the period of oyster deployment.

Denitrification Increases with Organic Matter Loading to Oxidized Sediments

Our study showed that denitrification enhancement in biodeposit-affected sediments is a function of bottom water DO and the rate of biodeposition. Denitrification rates were found to be higher in sediments receiving biodeposition than in control areas on all sampling dates. Consistent with previous findings of seasonality (Fulweiler et al. 2013; Piehler and Smyth 2011), denitrification rates were highest in July/August. Interannual differences in summer and fall denitrification rates indicated that sediment redox conditions also influenced CND rates.

Denitrification rates were partially controlled by sediment oxidation status with higher rates observed when bottom water DO was greater than 5 mg L^{-1} and the sediment surface showed a clearly visible oxidized surface. Time series DO records showed periodic basin-wide water column hypoxia at some point during each of the 3 years of study, with the timing, frequency, and duration of hypoxia being comparable between years. Sediments collected within the area receiving biodeposition in late summer 2017 were characterized by areas of surficial sulfidic sediments and shallow/poorly defined RPD depth due to the "extra" organic matter loading. Denitrification was not significantly enhanced on these occasions. In fact, cores with little or no visible surface oxidization had lower than expected denitrification rates despite greater N deposition compared to cores collected outside of the biodeposit area, which maintained an oxidized surface. Furthermore, cores within the biodeposit area that had a well-defined oxic layer had the highest enhanced denitrification rates during the study (i.e., July 2018; Table 5). Studies have demonstrated that oxygen is required for nitrification and CND are diminished or inhibited in sulfidic sediments (Fenchel et al. 1998; Joye and Hollibaugh 1995). The degree of inhibition is determined by the porewater sulfide concentration, and duration and frequency of exposure of the nitrifying and denitrifying microbial community to sulfides (Caffrey et al. 2019). From a management perspective, it is important to emphasize that predictions of N removal via denitrification will be an overestimate if surficial sediments are sulfidic.

Denitrification efficiencies (denitrification as % of total N mineralization) remained relatively constant across a range of organic matter loading rates but varied temporally. Biodeposits from floating oyster aquaculture appeared to increase denitrification rates and total N regeneration proportionally, as seen in the similar denitrification efficiencies in biodeposit affected and background sediments. However, denitrification efficiencies varied between seasons and years and were significantly affected by sediment oxidation status due to the reduction of denitrification in sulfidic sediments. Efficiencies were highest in spring, and the year 1 spring flux was the highest recorded (Table 5). Spring efficiencies were similar to findings by Owens (2009), who reported spring flux denitrification efficiencies > 50%. Efficiencies were lowest in summer when NH_4^+ production was highest.

A key finding of this study is that biodeposition increases the rate of sediment denitrification, and that the extent of the increase depends upon the rate of deposition to the sediment surface, as long as the surficial sediments remain oxidized. Significant positive linear relationships between N deposition and denitrification suggest the potential for modeled N deposition to predict CND in estuaries when this condition is met. When this condition is not met, such as when summer stratification of the water column results in hypoxic bottom waters, the remineralization of organic deposits results in a loss of the oxidized surface layer of the sediments, which inhibits CND. To this latter point, we note that in the present study, reduction in sediment denitrification was measured at the Lonnie's Pond aquaculture site at very high oyster densities (initial oyster densities per square meter of surface area were 224 oysters m^{-2}, 794 oysters m^{-2}, and 1852 oysters m^{-2} in 2016, 2017, and 2018, respectively) and where low bottom water oxygen conditions occasionally resulted in the loss of the surface oxidized layer, leading to sulfidic surficial sediments. Therefore, caution must be taken in floating aquaculture to not increase the stocking density to the point of causing bottom water hypoxia and reducing N loss via denitrification.

Maximizing N Removal from an Estuary via Floating Oyster Aquaculture

Our N mass balance reveals that floating oyster aquaculture enhances N removal via three pathways. Within the oyster system, oyster N assimilation (and subsequent removal from the system) accounts for the largest N removal, followed by CND enhancement, and then sediment N burial. This study quantified N removal via sediment burial, which enables a full accounting of N removal by oyster aquaculture; previous estimates typically include only N assimilation and

denitrification. Although the N burial component is small, it provides additional evidence that oyster activities, namely, biodeposition of labile organic matter, stimulate N removal and accelerate the entire N cycle. Permanent N removal through N assimilation and subsequent harvest (oyster removal from the system at the end of the growing season) was significantly greater than N removal via enhanced dinitrogen gas production. This suggests that oyster deployments can maximize N assimilation by maximizing growth rate, and that denitrification can be maximized by sustaining oxidized surficial sediments. Aquaculture practices such as deployment and removal dates, initial oyster size, stocking density, gear type, maintenance activities, and deployment location and orientation relative to flow patterns can all influence oyster production (Ferreira et al. 2007) and N removal via assimilation (Kellogg et al. 2014; Rose et al. 2015). In the present study, N removed via assimilation only increased 5% from year 1 to year 2 despite a 200% increase in population size and 31% increase in deployment duration (Table 6). Farm-scale ecosystem models suggest that there is a site-specific optimal stocking density and deployment area configuration for all potential aquaculture sites, including Lonnie's Pond, which maximizes growth rates without maximizing biodeposit or ammonia release (Ferreira et al. 2007). However, the usefulness of models to optimize an ecosystem service is potentially limited by the number and quality of the inputs and site-specific characteristics.

Conclusions

We quantified permanent N removal associated with floating oyster aquaculture in a small tidal salt pond on Cape Cod, southeastern MA. The results of this study suggest that when oysters are added to an estuary, their activities alter N cycling by accelerating the transfer of organic matter from the water column to the associated sediment area (biodeposit area) leading to increased sediment respiration. Without oysters, organic matter in the form of phytoplankton eventually settles to the bottom or is flushed from the estuary via the tidal outlet. We showed that denitrification increases with increasing N deposition in sediments that maintain an oxic surface layer. The N mass balance of the floating oyster aquaculture system indicates that the largest component of N removal is via assimilation into oyster tissue and shell and subsequent oyster removal from the system, followed by denitrification, and then burial. Nitrogen assimilation and denitrification were directly measured in this study. Enhanced denitrification (denitrification over background) within the sediment area receiving oyster biodeposits contributed an additional 27.9% removal of N from the system beyond that assimilated by oysters within their shells and tissue at time of removal from the system. Quantification of oyster-associated denitrification requires measurements both within the growing season and in the following spring, as labile biodeposits overwinter and continue to support denitrification into the following year. Site-specific aquaculture management practices (e.g., oyster deployment timing and oyster stocking density) can optimize oyster production of market-sized oysters, as well as increase biomass, which in turn increases N incorporated into tissue and shell over the growing season. These practices should support organic matter loading to sediments without affecting sediment redox conditions. Overall, the present study has showed that floating oyster aquaculture can significantly enhance permanent N removal primarily through denitrification and oyster harvest.

Acknowledgements The authors would like to thank the United States Environmental Protection Agency Southeast New England Program and the Town of Orleans for supporting this work. We gratefully acknowledge Science Wares Inc. for maintaining the oyster arrays and their assistance determining oyster survival, growth, and nitrogen assimilation and D.R. Schlezinger, J. Benson, S. Horvet, A. Unruh, and N. Uline of the Coastal Systems Program at SMAST-UMD. Special thanks to Dr. Mark Altabet for use of the MC-IRMS, which is part of the Stable Isotope Facility at UMassD/SMAST. We would also like to extend our gratitude to the two anonymous reviewers whose comments significantly improved this manuscript.

References

An, S., and W. Gardner. 2002. Dissimilatory nitrate reduction to ammonium (DNRA) as a nitrogen link, versus denitrification as a sink in a shallow estuary (Laguna Madre/Baffin Bay, Texas). *Marine Ecology Progress Series* 237: 41–50. https://doi.org/10.3354/meps237041.

Ayvazian, S., K. Mulvaney, C. Zarnoch, M. Palta, J. Reichert-Nguyen, S. McNally, M. Pilaro, A. Jones, C. Terry, and R.W. Fulweiler. 2021. Beyond bioextraction: The role of oyster-mediated denitrification in nutrient management. *Environmental Science and Technology* 55: 14457–14465.

Bayne, B.L., and A.J.S. Hawkins. 1992. Ecological and physiological aspects of herbivory in benthic suspension-feeding molluscs. In *Plant-animal interactions in the marine benthos*, ed. D. M. John, S. J. Hawkins, and J. H. Prince, 46th ed., 265–388. Oxford: Clarendon.

Caffrey, J.M., S. Bonaglia, and D.J. Conley. 2019. Short exposure to oxygen and sulfide alter nitrification, denitrification, and DNRA activity in seasonally hypoxic estuarine sediments. *FEMS Microbiology Letters*. https://doi.org/10.1093/femsle/fny288.

Charoenpong, C.N., L.A. Bristow, and M.A. Altabet. 2014. A continuous flow isotope ratio mass spectrometry method for high precision determination of dissolved gas ratios and isotopic composition. *Limnology and Oceanography: Methods* 12: 323–337. https://doi.org/10.4319/lom.2014.12.323.

Comeau, L.A. 2013. Suspended versus bottom oyster culture in eastern Canada: Comparing stocking densities and clearance rates. *Aquaculture* 410–411: 57–65. https://doi.org/10.1016/j.aquaculture.2013.06.017.

D'Elia, C.F., P.A. Steudler, and N. Corwin. 1977. Determination of total nitrogen in aqueous samples using persulfate digestion. *Limnology and Oceanography* 22: 760–764. https://doi.org/10.4319/lo.1977.22.4.0760.

Engström, P., T. Dalsgaard, S. Hulth, and R.C. Aller. 2005. Anaerobic ammonium oxidation by nitrite (anammox): Implications for N_2 production in coastal marine sediments. *Geochimica Et*

Cosmochimica Acta 69: 2057–2065. https://doi.org/10.1016/j.gca.2004.09.032.

Fenchel, T., G.M. King, and T.H. Blackburn. 1998. *Bacterial biogeochemistry: The ecophysiology of mineral cycling*. London: Academic Press.

Ferreira, J.G., A.J.S. Hawkins, and S.B. Bricker. 2007. Farm-scale assessment of shellfish aquaculture in coastal systems—the Farm Aquaculture Resource Management (FARM) model. *Aquaculture* 264: 160–174. https://doi.org/10.1016/j.aquaculture.2006.12.017.

Fulweiler, R.W., S.M. Brown, S.W. Nixon, and B.D. Jenkins. 2013. Evidence and a conceptual model for the co-occurrence of nitrogen fixation and denitrification in heterotrophic marine sediments. *Marine Ecology Progress Series* 482: 57–68. https://doi.org/10.3354/meps10240.

Hamersley, M., and B. Howes. 2005. Coupled nitrification-denitrification measured *in situ* in a *Spartina alterniflora* marsh with a $^{15}NH^{4+}$ tracer. *Marine Ecology Progress Series* 299: 123–135. https://doi.org/10.3354/meps299123.

Higgins, C., C. Tobias, M. Piehler, A. Smyth, R. Dame, K. Stephenson, and B. Brown. 2013. Effect of aquacultured oyster biodeposition on sediment N_2 production in Chesapeake Bay. *Marine Ecology Progress Series* 473: 7–27. https://doi.org/10.3354/meps10062.

Howarth, R.W., A. Sharpley, and D. Walker. 2002. Sources of nutrient pollution to coastal waters in the United States: Implications for achieving coastal water quality goals. *Estuaries* 25: 656–676. https://doi.org/10.1007/BF02804898.

Howes B., S.W. Kelley, J.S. Ramsey, R. Samimy, D. Schlezinger, E. Eichner (2006). Linked watershed-embayment model to determine critical nitrogen loading thresholds for Pleasant Bay, Chatham, Massachusetts. Massachusetts Estuaries Project, Massachusetts Department of Environmental Protection. Boston, MA.

Humphries, A.T., S.G. Ayvazian, J.C. Carey, B.T. Hancock, S. Grabbert, D. Cobb, C.J. Strobel, and R.W. Fulweiler. 2016. Directly measured denitrification reveals oyster aquaculture and restored oyster reefs remove nitrogen at comparable high rates. *Frontiers in Marine Science* 3: 41–50. https://doi.org/10.3389/fmars.2016.00074.

Jorgensen, C.B. 1975. Comparative physiology of suspension feeding. *Annual Review of Physiology* 37: 57–79. https://doi.org/10.1146/annurev.ph.37.030175.000421.

Joye, S.B., and J.T. Hollibaugh. 1995. Influence of sulfide inhibition of nitrification on nitrogen regeneration in sediments. *Science* 270: 623–625. https://doi.org/10.1126/science.270.5236.62.

Kellogg, M.L., J.C. Cornwell, M.S. Owens, and K.T. Paynter. 2013. Denitrification and nutrient assimilation on a restored oyster reef. *Marine Ecology Progress Series* 480: 1–19. https://doi.org/10.3354/meps10331.

Kellogg, M.L., A.R. Smyth, M.W. Luckenbach, R.H. Carmichael, B.L. Brown, J.C. Cornwell, M.F. Piehler, M.S. Owens, D.J. Dalrymple, and C.B. Higgins. 2014. Use of oysters to mitigate eutrophication in coastal waters. *Estuarine, Coastal and Shelf Science* 151: 156–168. https://doi.org/10.1016/j.ecss.2014.09.025.

Koop-Jakobsen, K., and A.E. Giblin. 2009. Anammox in tidal marsh sediments: The role of salinity, nitrogen loading, and marsh vegetation. *Estuaries and Coasts* 32: 238–245.

Kristen, W. 1983. *Organic Elemental Analysis: Ultramicro, Micro, and Trace Methods*. New York: Academic Press/Harcourt Brace Jovanovich.

Labrie, M.S., M.A. Sundermeyer, and B.L. Howes. 2022. Modelling the spatial distribution of oyster (*Crassostrea virginica*) biodeposits settling from suspended aquaculture. *Estuaries and Coasts*. https://doi.org/10.1007/s12237-022-01096-4.

Lohrenz, S.E., C.D. Taylor, and B.L. Howes. 1987. Primary production of protein: 2. Algal protein metabolism and its relation to particulate organic matter composition in the surface mixed layer. *Marine Ecology Progress Series* 40: 175–183.

Lunstrum, A., K. McGlathery, and A. Smyth. 2018. Oyster (*Crassostrea virginica*) Aquaculture shifts sediment nitrogen processes toward mineralization over denitrification. *Estuaries and Coasts* 41 (4): 1130–1146. https://doi.org/10.1007/s12237-017-0327-x.

Magni, P., S. Montani, C. Takada, and H. Tsutsumi. 2000. Temporal scaling and relevance of bivalve nutrient excretion on a tidal flat of the Seto Inland Sea, Japan. *Marine Ecology Progress Series* 198: 139–155. https://doi.org/10.3354/meps198139.

Murphy, J., and J.P. Riley. 1958. A single-solution method for the determination of soluble phosphate in sea water. *Journal of the Marine Biological Association of the United Kingdom* 37: 9–14. https://doi.org/10.1017/S0025315400014776.

Newell, R.I.E., and S.J. Jordan. 1983. Preferential ingestion of organic material by the American oyster *Crassostrea virginica*. *Marine Ecology Progress Series* 13: 47–53. https://doi.org/10.3354/meps013047.

Oudot, C., R. Gerard, P. Morin, and I. Gningue. 1988. Precise shipboard determination of dissolved oxygen (Winkler procedure) for productivity studies with a commercial system. *Limnology and Oceanography* 33: 146–150.

Owens, M.S. 2009. *Nitrogen Cycling and Controls on Denitrification in Mesohaline Sediments of Chesapeake Bay*. Master's Thesis: University of Maryland, College Park, MD, USA.

Piehler, M.F., and A.R. Smyth. 2011. Habitat-specific distinctions in estuarine denitrification affect both ecosystem function and services. *Ecosphere* 2: 1–17. https://doi.org/10.1890/ES10-00082.1.

Ray, N.E., B. Hancock, M.J. Brush, A. Colden, J. Cornwell, M.S. Labrie, T.J. Maguire, T. Maxwell, D. Rogers, R.J. Stevick, and A. Unruh. 2021. A review of how we assess denitrification in oyster habitats and proposed guidelines for future studies. *Limnology and Oceanography: Methods* 19 (10): 714–731.

Reitsma, J., D. Murphy, and A. Franklin. 2014. *Shellfish nitrogen content from coastal waters of southeastern Massachusetts*. Ext: Woods Hole Sea Grant Cape Cod Coop.

Rich, J.J., O.R. Dale, B. Song, and B.B. Ward. 2008. Anaerobic ammonium oxidation (anammox) in Chesapeake Bay sediments. *Microbial Ecology* 55: 311–320. https://doi.org/10.1007/s00248-007-9277-3.

Rose, J.M., S.B. Bricker, and J.G. Ferreira. 2015. Comparative analysis of modeled nitrogen removal by shellfish farms. *Marine Pollution Bulletin* 91: 185–190. https://doi.org/10.1016/j.marpolbul.2014.12.006.

Rose, J.M., J.S. Gosnell, S. Bricker, M.J. Brush, A. Colden, L. Harris, E. Karplus, A. Laferriere, N.H. Merrill, T.B. Murphy, and J. Reitsma. 2021. Opportunities and challenges for including oyster-mediated denitrification in nitrogen management plans. *Estuaries and Coasts* 44: 2041–2055.

Rudnick, D.T., and C.A. Oviatt. 1986. Seasonal lags between organic carbon deposition and mineralization in marine sediments. *Journal of Marine Research* 44: 815–837. https://doi.org/10.1357/002224086788401594.

Scheiner, D. 1976. Determination of ammonia and Kjeldahl nitrogen by indophenol method. *Water Research* 10: 31–36. https://doi.org/10.1016/0043-1354(76)90154-8.

Smyth, A.R., S.P. Thompson, K.N. Siporin, W.S. Gardner, M.J. McCarthy, and M.F. Piehler. 2013. Assessing nitrogen dynamics throughout the estuarine landscape. *Estuaries and Coasts* 36 (1): 44–55. https://doi.org/10.1007/s12237-012-9554-3.

Songsangjinda, P., O. Matsuda, T. Yamamoto, N. Rajendran, and H. Maeda. 2000. The role of suspended oyster culture on nitrogen cycle in Hiroshima Bay. *Journal of Oceanography* 56: 223–231. https://doi.org/10.1023/A:1011143414897.

Srna, R.F., and A. Baggaley. 1976. Rate of excretion of ammonia by the hard clam *Mercenaria* and the American oyster *Crassostrea virginica*. *Marine Biology* 36: 251–258. https://doi.org/10.1007/BF00389286.

Town of Orleans Water Quality and Wastewater Planning. 2018. *Amended Comprehensive Wastewater Management Plan – Final*. Pocasset: AECOM Technical Services Inc.

Wood, E.D., F. Armstrong, and F.A. Richards. 1967. Determination of nitrate in sea water by cadmium-copper reduction to nitrite. *Journal of the Marine Biological Association of the United Kingdom* 47: 23–31. https://doi.org/10.1017/S002531540003352X.